WETTING LAYER EVOLUTION AND INTERFACIAL HEAT TRANSFER IN WATER-AIR SPRAY COOLING PROCESS OF HOT METALLIC SURFACE

by

Lidan NING, Liping ZOU, Zhichao LI, and Huiping LI [a*]

School of Materials Science and Engineering,
Shandong University of Science and Technology, Qingdao, Shandong, China

Original scientific paper
https://doi.org/10.2298/TSCI210615318N

Spray cooling experiments on the hot metallic surfaces with different initial temperatures were performed. This paper adopts a self-developing program which is based on the inverse heat transfer algorithm to solve the interfacial heat transfer coefficient and heat flux. The temperature-dependent interfacial heat transfer mechanism of water-air spray cooling is explored according to the wetting layer evolution taken by a high speed camera and the surface cooling curves attained by the inverse heat transfer algorithm. Film boiling, transition boiling, and nucleate boiling stages can be noticed during spray cooling process of hot metallic surface. When the cooled surface's temperature drops to approximately 369-424 °C. the cooling process transfers into the transition boiling stage from the film boiling stage. The wetting regime begins to appear on the cooled surface, the interfacial heat transfer coefficient and heat flux begin to increase significantly. When the cooled surface's temperature drops to approximately 217-280°C, the cooling process transfers into the nucleate boiling stage. The cooled surface was covered by a liquid film, and the heat flux begins to decrease significantly.

Key words: *water-air spray cooling, interfacial heat transfer characteristics, wetting layer evolution*

Introduction

Spray cooling is a high effeciency heat transfer technology that atomizes the cooling medium through a nozzle with high pressure gas or its own pressure, and then sprays it on the surface of the cooled part at a certain speed. The heat is taken away from the surface of a cooled object through the single phase and the two-phase heat exchange [1-4]. Compared with other quenching processes, spray cooling technology has the characteristics of high heat exchange capacity, good uniformity of heat removal, no pollution the environment, and no contact thermal resistance with overheat surface [5-7]. Spray cooling has a broad application prospect in heat dissipation with high heat flux [8-10].

Spray cooling of hot steel surfaces is an indispensable part of continuous casting and heat treatment [11, 12]. The spray cooling rate must be dynamically controlled to maintain competitiveness and continuously produce high strength, high quality steel at the highest productivity during continuous casting. Besserer *et al.* [13] adopt orbital forming method to manufacture semi-finished parts which are used DP600 deep-drawing steel as the material,

[*] Corresponding author, e-mail: lihuiping99@163.com

and perform surface heat treatment on parts. The results showed that a proper water-air spray cooling process could induce compressive stresses which is conductive to improve fatigue life. Gretzki *et al.* [14] believe that water-air spray cooling is very effective for carrying out surface hardening on die-forged components. Rodman *et al.* [15] adopt a water-air spray cooling to surface hardening spur gearwheels which are made of $42CrMo_4$ hardening and tempering steel. The results show that the distortion is evenly distributed, which indicates that the wetting behavior of the spray cooling is homogeneous. Spray cooling quenching is an up-and-coming method of quenching Al-Mg-Si alloys. By adjusting the pressure ratio of air to water, the final temperature of the profile can have a wide adjustment range which can minimize the temperature gradient of the complex profiles and reduce the deformation of the profile [16].

During the spray cooling process, it is essential to remove heat efficiently and uniformly without cracking or distorting the slab. It is challenging to obtain an accurate heat transfer coefficient (HTC) on the surface of the slab and employ the obtained HTC as the boundary condition of the solidification calculation [17]. The temperature-dependent interfacial heat transfer coefficient (IHTC), properties of the extruded profile, and the spray cooling parameters can be decided employing the lumped heat capacitance method and other methods [18]. The spray cooling process from the surface temperature of about 1200 °C to the Leidenfrost point (LFP) temperature was studied [19]. The 1-D sequential Beck's approach [20, 21] was employed to estimate the heat fluxes, the surface temperatures, and the IHTC. Abed *et al.* [22] studied transient heat transfer based on the lumped capacitance model and evaluated the heat transfer behavior of water-air droplets two-phase flow. Hadała *et al.* [23] investigated the air-atomized water spray cooling of vertical plates and developed a model related to the local HTC, which is a function of pressure, surface temperature, and spray height.

Overviewing the previous literature, the system study of initial temperature effect on IHTC, LFP, heat flux, and wetting layer evolution has not been present in water-air spray cooling. The LFP is essential for the quenching of metal alloys because it is a symbol of the transition from inferior heat transfer in film boiling to the very superior heat transfer related to transition boiling [24]. Now that rapid quenching is crucial to achieve excellent mechanical properties of materials, it is also essential to precisely predict and control the LFP. Even if the LFP has a clear definition, it is (in the case of spray cooling) challenging to automatically read it from experiment data [11]. In this research, the water-air spray cooling of a hot metallic surface with different initial temperatures (600 °C, 650 °C, 700 °C, 750 °C, 800 °C, 850 °C, and 900 °C) is studied. A self-developing software based on the improved advance and retreat method and golden section method is adopted to solve the transient surface parameters, for instance, the IHTC, heat flux, cooling curves*, etc.* According to the evolution of the wetting layer captured by the high speed camera and the transient surface parameters, the temperature-dependent interfacial heat transfer mechanism of water-air spray cooling is explored. The LFP is determined according to the wetting layer evolution and surface temperature, IHTC, and heat flux. This research discusses the influence of initial temperatures on the heat transfer characteristics.

Experimental description

Spray cooling set-up

Water-air spray cooling experiments were performed adopting the spray cooling set-up shown in fig. 1(a). Austenitic stainless steel (AISI 304) was chosen for the studies to avert the release of latent heat. The dimensions of the sample are shown in fig. 1(b). The diameter of the hole used to measure temperature by the thermocouple is 1.5 mm. The main components consist of an induction heating device, water reservoir, fluid-flow meter, air compressor, gas-flow meter, data acquisition system, and nozzle, fig. 1(c).

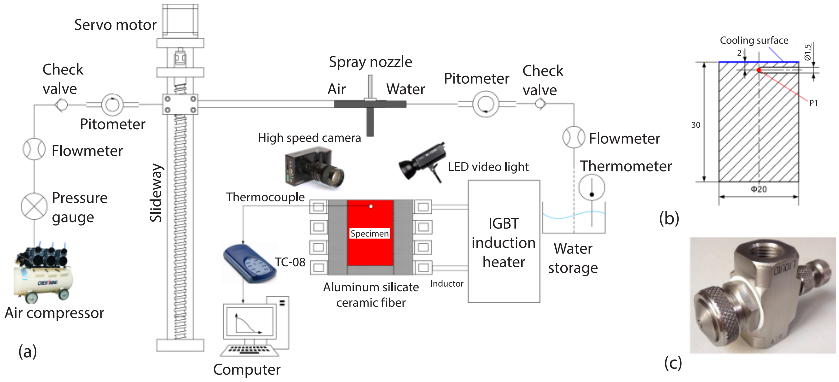

Figure 1. Schematic diagram of the experimental set-up

The samples are heated by an IGBT induction heating device. The heating time is very short, and the oxidation on the sample surface is not apparent. Therefore, the impact of the oxide layer on the heat transfer is ignored when discussing the interfacial heat transfer characteristics in this study. The cooling curves of the P1 position, as depicted in fig.1(b), are recorded in the cooling process by the *K*-type armored thermocouples, temperature recorder TC-08 and PicoLog data acquisition software. The acquisition interval (sampling frequency) is 400 ms. The Chronos 1.4 high speed camera is used to record the wetting layer evolution on the cooling surface of the sample in the cooling process. The resolution of Chronos 1.4 is set up to 1280×1024, and the frame rate is 1000 fps. During capturing the high speed video, two Godox SL-100W LED video lights are used as light sources. Its light intensity can be regulable and it is completely flicker-free from 33-100% output.

The nozzle is fixed on the guide rail, the nozzle inclination is 0°, and the spray height is set to 80 mm. The sample is wrapped with the high aluminum silicate ceramic fiber paper and placed into the induction coil with an inner diameter of 50 mm. Insert a thermocouple into the sample's hole for the measurement of temperature. The air pressure is adjusted to 0.2 MPa. The water and air-flows are measured by the fluid-flow meter and the gas-flow meter, respectively. The water temperature is about 25 °C. The air pressure is 0.2 MPa, the flow rate is approximately 63 Lpm. Multiple experiments for each initial temperature are performed to ensure the reliability of the experimental results.

Uncertainty analysis

In the current research, efforts are made to reduce the uncertainty in the experimental and inverse heat transfer calculation results to maximize the reliability of the research results. The main uncertainty is that the *K*-type thermocouple is adopted to measure the actual time temperature data in the experiment. The uncertainty of the full scale of the *K*-type thermocouple is ±0.4%. The temperature measurement accuracy for *K*-type thermocouple is approximately ±1.5 °C. The USB TC-08 data acquisition device has a high resolution (20 bit) and high precision (±0.2% reading and ±0.5 °C). According to the law of error propagation [25], the uncertainty of temperature measurement resulted from the *K*-type thermocouples and data acquisition device is ±1.58 °C.

Experimental results and analysis

Inverse heat transfer analysis

The thermal analysis was carried out by using an inverse heat conduction algorithm for the estimation of surface temperature, IHTC, and heat flux. The thermal insulation material's thermal conductivity is 0.037-0.055 $Wm^{-1}°K^{-1}$ [26]. The thickness of aluminum silicate ceramic fiber paper is approximately 15 mm. Depending on the definition of HTC and thermal conductivity, the HTC of a certain thickness of insulating material can be roughly calculated. The HTC is roughly equal to thermal conductivity divided by the thickness of the material, so the HTC between sample and atmosphere is about 2.47-3.67 $Wm^{-2}°C^{-1}$. Compared to the spray cooling surface, the cooling rate of insulating layer is very slow, which minimizes the radial heat loss of the sample and makes the heat transfer approximately 1-D. Therefore, when studying spray heat transfer from the top surface of the sample, this research regards it as 1-D heat transfer [27]. The validity of the 1-D assumption has been validated [28].

The heat conduction equation, initial condition, and boundary conditions can be described as eqs. (1)-(4), respectively:

$$\rho c_p \frac{\partial T}{\partial t} = \frac{\partial}{\partial z}\left(\lambda \frac{\partial T}{\partial z}\right) \tag{1}$$

where T [°C] is the temperature, ρ [kg^{-3}] – the density, c_p [$Jkg^{-1}°C^{-1}$] – the specific heat capacity, λ [$Wm^{-1}°K^{-1}$] – the thermal conductivity, t [s] – the time, and z – the co-ordinate along the axial direction of the sample.

Initial condition:

$$T|_{t=0} = f(z) \tag{2}$$

For boundary conditions, all surfaces except for the cooled surface are assumed to be adiabatic boundary conditions:

$$-\lambda \frac{\partial T}{\partial z}|_{z=0} = q(t) = H(T - T_f) \text{ at the cooling surface} \tag{3}$$

$$\frac{\partial T}{\partial z}|_{z} = 0 \text{ at other surface} \tag{4}$$

where q [Wm^{-2}] is the surface heat flux, which is a function of time, t, H [$Wm^{-2}°C^{-1}$] – the IHTC, which is a function of temperature, and T_f – the temperature of water-air spraying.

According to the temperature data measured in the experiment, the surface temperature, IHTC, and surface heat flux are solved through a self-developing inverse heat transfer program [26, 29] based on the improved advance and retreat method and golden section method. The efficiency, accuracy, and convergence of the inverse heat transfer program have been confirmed in the references [26, 29]. Table 1 shows the thermal conductivity and specific heat of 304 stainless steel [30].

Table 1. The thermal conductivity and specific heat of 304 stainless steel

Temperature [°C]	20	100	200	300	400	500	600	700	800	900	1000
Conductivity [$Wm^{-1}K^{-1}$]	11.9	12.6	13.6	14.5	15.5	16.5	17.6	18.9	20.3	22.1	24.5
Specific heat [$Jkg^{-1}K^{-1}$]	476	483	491	500	508	518	529	543	562	588	626

In the experiments, the temperature curves at the P1 position, as shown in fig. 1(b), measured by the data acquisition system and thermocouple are demonstrated in fig. 2. In light of the temperature curves at the P1 position, the temperature curves on the cooling surface can be calculated by the inverse heat transfer program. The surface temperature curves are illustrated in fig. 3. The temperature curves in fig. 3 show that, for the samples with the initial temperatures of 600 °C, 650 °C, 700 °C, 750 °C, 800 °C, 850 °C, and 900 °C, all cooling curves have an obvious inflection point.

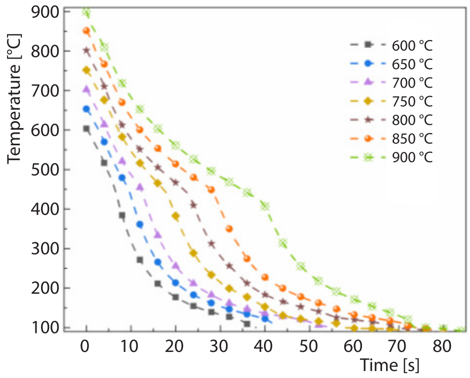

Figure 2. Measured temperature curves of P1 position for the samples with different initial temperatures

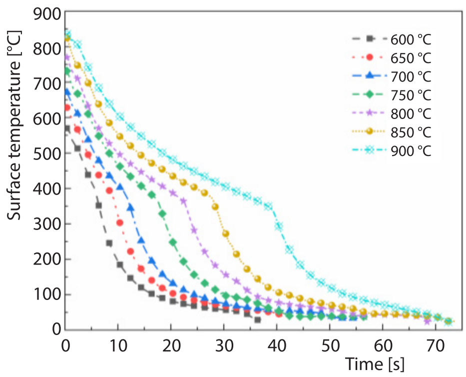

Figure 3. Surface temperature curves on the cooling surface of samples with different initial temperatures

According to the temperature curves of the P1 position shown in fig. 2, the IHTC and heat flux on the cooling surface of the sample can also be calculated by the inverse heat transfer method, as shown in figs. 4 and 5. As can be clearly seen from fig. 4, for all samples with the initial temperature of 600 °C, 650 °C, 700 °C, 750 °C, 800 °C, 850 °C, and 900 °C, when the surface temperatures of the sample are in the range of 400-900 °C, the IHTC increases gradually with the decrease of sample's surface temperature. When sample's surface temperature reduces to approximately 400 °C, the IHTC rises to approximately 2000 [$Wm^{-2}°C^{-1}$]. The curves of IHTC have an obvious inflection point and the IHTC begins to increase sharply. When sample's surface temperature reduces to about 100 °C, the IHTC can reach approximately 14000 [$Wm^{-2}°C^{-1}$].

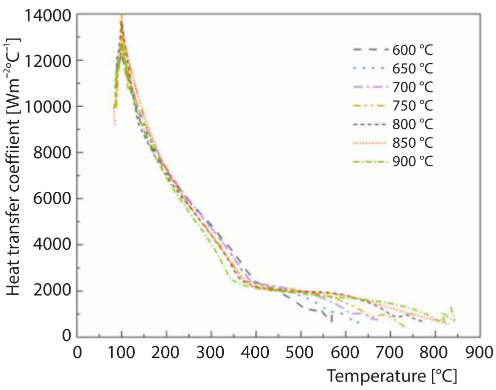

Figure 4. The IHTC on the cooling surface of samples

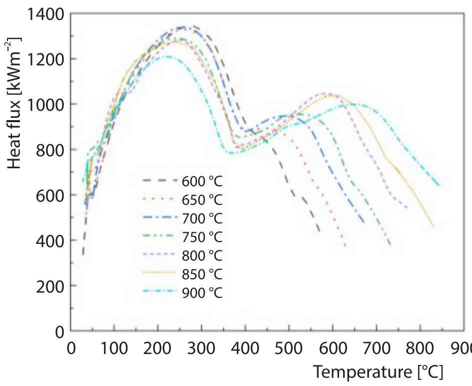

Figure 5. Surface heat flux on the cooling surface of samples

It can be seen from fig. 5, for all samples with the initial temperatures of 600 °C, 650 °C, 700 °C, 750 °C, 800 °C, 850 °C, and 900 °C, the tendency of heat flux curves is similar. When the surface temperatures of the samples are in the range of 400-900 °C, the surface heat flux of the samples grows rapidly at the initial cooling stage and then reduces gradually with the decrease of sample's surface temperature. When sample's surface temperature reduces to approximately 400 °C, there is an obvious inflection point on the surface heat flux curve of the sample. The surface heat flux begins to increase quickly and reaches the critical heat flux when the surface temperature reaches approximately 250 °C. The heat flux is in the range of 1100-1300 kW/m^2 at the critical point. When sample's surface temperature is lower than 250 °C, the surface heat flux begins to decreases.

Wetting layer evolution of cooling surface

The sample is heated up to the different initial temperatures (approximately 600 °C, 650 °C, 700 °C, 750 °C, 800 °C, 850 °C, and 900 °C), and then the sample surface is cooled by the water-air spray cooling. The wetting layer evolution of the surface with different initial temperatures is displayed in fig. 6. It can be clearly seen that there are three surface states (the dry state, the wetting state, and the transition state) on the cooling surface during the water-air spray

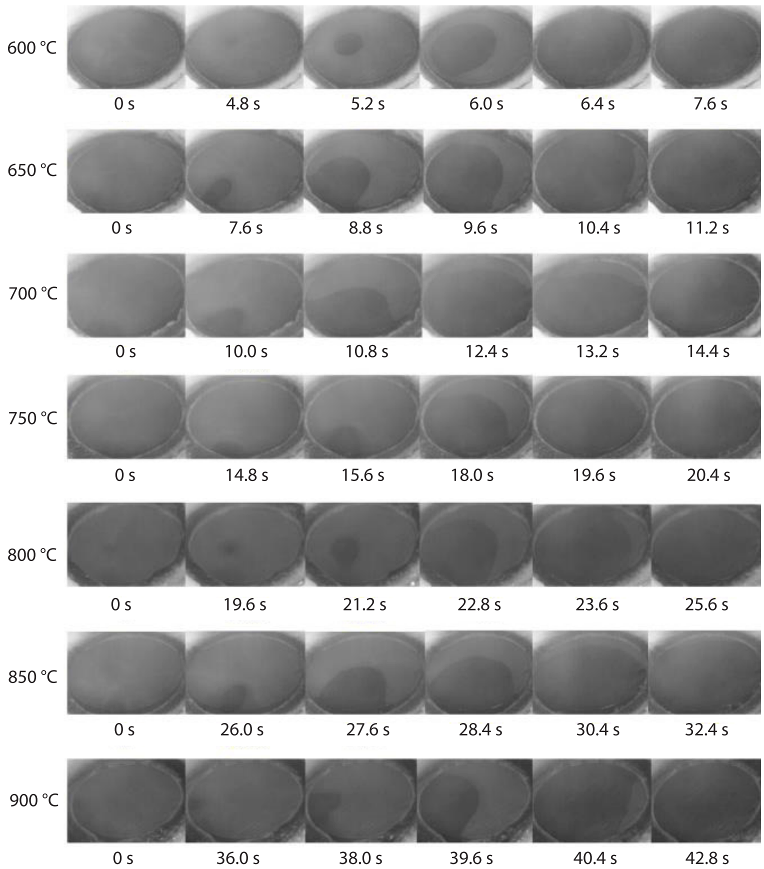

Figure 6. Wetting layer evolution of sample surface with the different initial temperatures

cooling. One is heat transfer with a dry surface layer, the other is heat transfer with a wetting surface layer, and another is heat transfer with the transition state between the dry layer and the wetting layer. The wetting layer can begin to appear on any position of the cooling surface and gradually expands until it covers the whole surface.

According to the wetting layer evolution taken by the high speed camera and the surface temperatures solved by the inverse heat transfer program, the finish temperatures of the dry surface layer (the onset temperatures of the wetting layer) for the samples with the initial temperature 600 °C, 650 °C, 700 °C, 750 °C, 800 °C, 850 °C, and 900 °C are approximately 424 °C, 410 °C, 408 °C, 402 °C, 395 °C, 387 °C, and 369 °C, respectively. This temperature is LFP [10], as shown in fig. 7. It is temperature at which the wetting area begins to appear on the hot metallic surface after the steam film ruptures, that is, the temperature at which the mechanism of heat transfer changes from film boiling to transition boiling [31]. For the surface with different initial temperatures, LFP is approximately in the range of 369-424 °C. The LFP gradually decreases with the increasing of the initial temperature.

The retention time of the dry surface layer is different for the surface with different initial temperatures. As the initial temperatures of samples are 600 °C, 650 °C, 700 °C, 750 °C, 800 °C, 850 °C, and 900 °C, the dry surface layer remains approximately 4.8 second, 7.6 seconds, 10 seconds, 14.8 seconds, 19.6 seconds, 26 seconds, and 36 seconds, respectively, as depicted in fig. 8. The higher the initial temperature is, the longer the retention time of the dry surface layer is. It means the time of film boiling rises with the increase of the initial temperature. In addition, the retention time of the transition state is different for the different initial temperatures, and it also grows with the rise of the initial temperature. As the initial temperatures of samples are 600 °C, 650 °C, 700 °C, 750 °C, 800 °C, 850 °C, and 900 °C, their transition states remained approximately 2.8 seconds, 3.6 seconds, 4.4 seconds, 5.6 seconds, 6 seconds, 6.4 seconds, and 6.8 seconds, respectively, as shown in fig. 8. Moreover, the temperature of the wetting surface layer covering the whole surface is different for the surface with different initial temperatures. This temperatures for the samples with the different initial temperature are approximately 280 °C, 265 °C, 252 °C, 248 °C, 242 °C, 223 °C, and 217 °C, respectively, which is in the range of 217-280 °C.

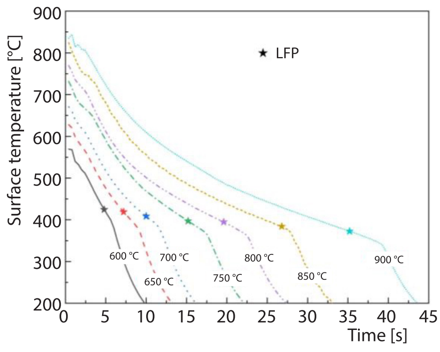

Figure 7. The LFP for the surface with different initial temperatures

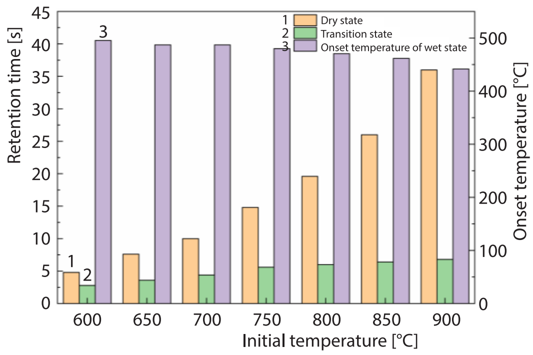

Figure 8. The retention time of the dry and transition state and the onset temperature of the wetting surface layer

Results and analysis

The cooling process of a hot metallic surface with different initial temperatures can be divided into five heat transfer regimes, such as convective heat transfer, nucleate boiling, transition boiling, film boiling, and vaporization.

In the early stage of water-air spray cooling, the tiny water droplets with the size of 0.02-0.1 mm contact the surface at high temperatures. Due to the higher initial temperature of the surface, there is a large temperature difference between the water droplets and the hot metallic surface. The tiny water droplets evaporate rapidly, and a lot of steam bubbles appear on the surface. Some steam bubbles at high pressure are expanding rapidly, and others steam bubbles at low pressure after expanding are disappearing. However, there are not enough droplets, and the steam from the evaporation of water droplets cannot form a complete vapor film on the surface. The heat transfer between the hot metallic surface and water spraying is mainly by the evaporation of water droplets. The surface heat flux rises sharply due to the increase of the water droplets contacting the hot metallic surface, as shown in fig. 5. The evaporation process of water droplets sprayed on the hot metallic surface is depicted in fig. 9.

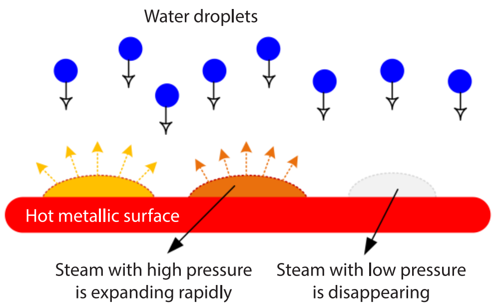

Figure 9. Evaporation process of water droplets sprayed on the hot metallic surface

When there are enough water droplets sprayed on the hot metallic surface, the steam from the vaporization of a large number of water droplets forms a complete high pressure steam film on the hot metallic surface. The heat exchange between the hot metallic surface and water spraying is mainly by the film boiling. Because of the blocking of the high pressure and high temperature steam film, it is difficult for the droplets in the water spraying to contact the hot metallic surface, and the hot metallic surface exhibits a dry state.

The saturated steam pressure can be calculated by the Antoine equation [32]:

$$\log_{10} P_s = A - B/(T + C) \tag{5}$$

where P_s [mmHg] is the saturated steam pressure, T [°C] – the temperature, and A, B, and C are Antoine coefficients.

If the temperature is in the range of 0.01-373.98 °C, A = 8.05573, B = 1723.6425, C = 233.08. As T = 373.98 °C, P_s is equal to 21.9 MPa according to eq. (5), which is far more than 0.2 MPa. Experimental results show that the temperature from the film boiling to the transition boiling is greater than 373.98 °C. According to Antoine equation, the higher the temperature, T, the greater the pressure, P_s. Therefore, it is more difficult for the tiny water droplets to contact the hot metallic surface at the stage of film boiling.

The tiny water droplets with high turbulence and high momentum may penetrate the vapor film, but they are evaporated before hitting the hot metallic surface because of the high temperature and pressure in the vapor film. The tiny water droplets are transformed into the vapor bubbles in the vapor film, as shown in fig. 10. The heat energy on the hot metallic surface is slowly transferred to the vapor film and the water spraying mainly by the thermal radiation. Vapor from the evaporation of water droplets is beneficial to maintain the vapor film on the hot metallic surface. The heat energy from the hot metallic surface is helpful to keep the high temperature of vapor film. The heat exchange by the thermal radiation in the vapor film is much less than the convective heat transfer. The IHTC and the surface heat flux are small at the stage of film boiling, as shown in figs. 4 and 5.

The temperature of the hot metallic surfaces becomes lower and lower in the water-air spray cooling. When the temperature difference between the hot metallic surface and the water spraying cannot maintain a complete vapor film, the vapor film on the surface begins to crack from an uncertain location. The rupture region of vapor film is getting larger and larger, as shown in fig. 6. In the rupture region of vapor film, some tiny water droplets begin to gather on the surface of the metallic sample and form the larger water droplets. The water droplets directly contact with the surface, and the wet region begins to appear. With the increase of the rupture area of vapor film, the wet region increases gradually. Eventually, the wet region covers the surface of the metallic sample completely.

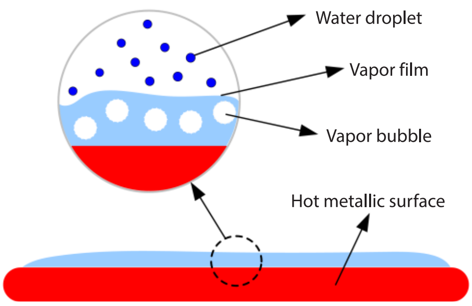

Figure 10. Sketch of film boiling on the hot metallic surface

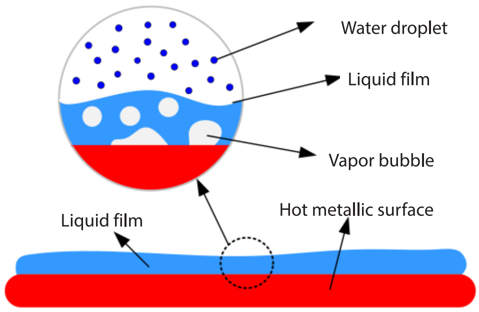

Figure 11. Sketch of transition boiling on the hot metallic surface

At the stage of transition boiling, the heat exchange on the metallic surface with the dry region is similar to that of film boiling, and the heat energy is transferred to the vapor film, and the water spraying mainly by the thermal radiation. For the surface with the wet region, many tiny water droplets continuously fell into the wetting layer. At the same time, the wetting layer close to the hot metallic surface vaporizes rapidly. Vapor produce on the surface and then escapes quickly from the surface in the form of vapor bubbles, as shown in fig. 11. A lot of heat energy is taken away from the hot metallic surface by the vaporization and convective heat transfer. The heat flux from the metallic surface begins increasing. Unlike the film boiling, the discontinuous bubbles on the wall can make the water contact the surface. The formation, growth, and rupture of bubbles have an interference effect on the wall film, and the efficiency of heat transfer is the highest [27]. The cooling rate on the surface is faster, the IHTC and the surface heat flux increase rapidly, as shown in figs. 4 and 5.

As the temperature of the metallic surface is further reduced, the temperature difference between the metallic surface and the water spraying cannot keep the boiling film at the stage of transition boiling, and then nucleate boiling starts. Nucleate boiling is characterized by a very high heat exchange rate at the metallic surface. Hundreds of tiny steam bubbles nucleate and grow at points on the metallic surface and detach from the surface, as shown in fig. 12. At this time, the metallic surface continues to maintain the wet state. Then the transition boiling ends, and nucleate boiling begins. As the nucleate boiling continues, the metallic surface is getting colder and colder, the heat flux from the metallic surface begins reducing, as shown in fig. 5. At the nucleate boiling stage, the metallic surface temperature slightly drops above the boiling temperature of water (100 °C).

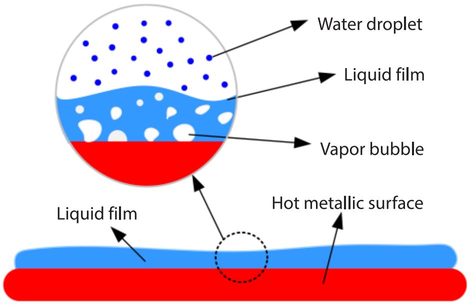

Figure 12. Sketch of nucleate boiling on the hot metallic surface

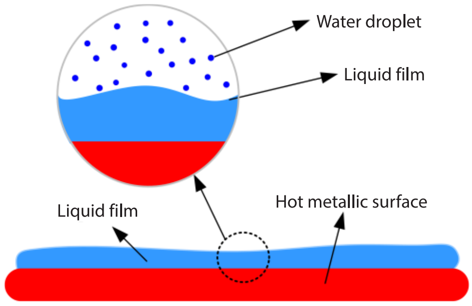

Figure 13. Sketch of single-phase convection on the hot metallic surface

As the metallic surface temperature is close to 100 °C, the heat flux from the surface cannot keep the nucleate boiling mode anymore. As the last cooling stage, convection (single-phase regime) begins, as shown in fig. 13.

For the hot metallic surface with the initial temperature of approximately 750 °C and 900 °C, the cooling curve, surface heat flux and the wetting layer evolution taken by the high speed camera are depicted in fig. 14. Comparing fig. 14(a) with fig. 14(b), it can draw a conclusion that the evolution of cooling surface, heat flux, and wetting layer are similar. Although the initial temperature is different, both of them include five stages: vaporization, film boiling, transition boiling, nucleate boiling, and single-phase convection.

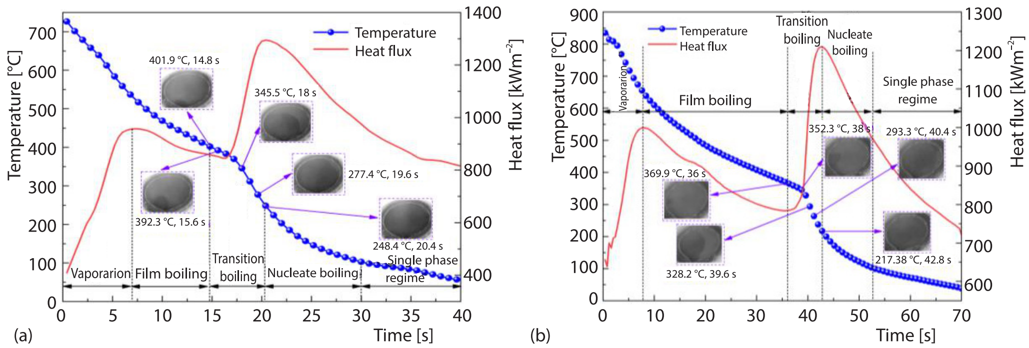

Figure 14. Cooling curve, heat flux, and the wetting layer evolution; (a) initial temperature at 750 °C and (b) initial temperature at 900 °C

Conclusions

The interfacial heat transfer characteristics of the hot metallic surface during the water-air spray cooling are investigated. The relationships among temperature curves, IHTC, and surface heat flux with different initial temperatures were analyzed. The conclusions are as follows.

- In the water-air spray cooling, the hot metallic surface at the initial temperature 600-900 °C appears the dry and wet states. The heat transfer on the surface includes five stages: vaporization, film boiling, transition boiling, nucleate boiling, and single-phase convection.
- The initial temperatures of samples slightly affect the LFP temperature. The LFP temperature gradually decreases with the initial temperature increase. As the initial temperatures are 600-900 °C, the LFP temperature is in the range of 424-369 °C.

- As the surface temperature is not less than the LFP temperature, the surface appears a dry state and heat transfer is mainly by film boiling. When the surface temperature reaches the LFP temperature, the wetting layer begins appearing on the surface, and gradually covers the whole surface. The retention time of film boiling rises with the increase of the initial temperatures.
- The initial temperatures have little influence on the HTC and heat flux. At the LFP temperature, the HTC is approximately 2000 W/m^2°C, and the heat flux can be about 800-900 kW/m^2.

Acknowledgment

This work was financially supported by the National Natural Science Foundation of China (52175342, 52005304), Natural Science Foundation of Shandong Province (ZR2021ME129).

Nomenclature

c_p – specific heat capacity, [Jkg^{-1}°C^{-1}]
H – interfacial heat transfer coefficient, [Wm^{-2}°C^{-1}]
P_s – saturated steam pressure, [mmHg]
q – surface heat flux, [Wm^{-2}]
T – temperature, [°C]
t – time, [second]
T_f – temperature of water-air spraying, [°C]
z – co-ordinate along the axial direction of the sample

Greek letters

λ – thermal conductivity, [Wm^{-1}K^{-1}]
ρ – density, [kgm^{-3}]

References

[1] Liu, R., *et al*., Applications of Spray Cooling Technology In Aerospace Field, *IOP Conf. Ser. Mater. Sci. Eng*., *470* (2019), 1, 012020
[2] Mohapatra, S. S., *et al*., Enhancement of Cooling Rate For A Hot Steel Plate Using Air-Atomized Spray With Surfactant-Added Water, *Exp. Heat Transf.*, *27* (2014), 1, pp. 72-90
[3] Nayak, S. K., Mishra, P. C., Thermal Characteristics of Air-Water Spray Impingement Cooling of Hot Metallic Surface under Controlled Parametric Conditions, *Journal Therm. Sci*., *25* (2016), 3, pp. 266-272
[4] Sardar, R., *et al*., Air-Water Mist Cooling Characteristics of an MS Plate in a Laboratory Scale ROT- an Experimental Observation, *Applied Mech. and Materials*, *903* (2021), Apr., pp. 45-49
[5] Kim, J., Spray Cooling Heat Transfer: The State of The Art, Int. *J. Heat Fluid-Flow*, *28* (2007), 4, pp. 753-767
[6] Malinowski, Z., *et al*., Inverse Method Implementation Heat Transfer Coefficient Determination over the Plate Cooled By Water Spray, *Inverse Probl. Sci. Eng*., *23* (2015), 3, pp. 518-556
[7] Mudawar, I., Assessment of High-Heat-Flux Thermal Management Schemes, *IEEE Trans. Components Packag. Technol*., *24* (2001), 2, pp. 122-141
[8] Liu, N., *et al.*, Experimental Investigation of Comprehensive Effects of Surfactant and Inclined Mode on Spray Cooling Heat Transfer, *Int. J. Therm. Sci*., *136* (2019), Oct., pp. 457-466
[9] Zhang, Z., *et al*., Experimental Investigation on Heat Transfer Characteristics of R1336mzz Flash Spray Cooling, *Appl. Therm. Eng*., *174* (2020), Mar., 115277
[10] Cai, C., *et al*., Theoretical Leidenfrost Point (LFP) Model for Sessile Droplet, *Int. J. Heat Mass Transf*., *146* (2020), 118802
[11] Hnizdil, M., *et al*., Prediction of Leidenfrost Temperature in Spray Cooling for Continuous Casting and Heat Treatment Processes, *Metals (Basel)*, *10* (2020), 11, 1551
[12] Wendelstorf, J., *et al*., Spray Water Cooling Heat Transfer at High Temperatures and Liquid Mass Fluxes, *Int. J. Heat Mass Transf*., *51* (2008), 19-20, pp. 4902-4910
[13] Besserer, H. B., *et al*., Induction Heat Treatment of Sheet-Bulk Metal-Formed Parts Assisted By Water-Air Spray Cooling, *Steel Res. Int*., *87* (2016), 9, pp. 1220-1227
[14] Gretzki, T., *et al*., Manufacturing Surface Hardened Components of 42CrMo4 By Water-Air Spray Cooling, *Steel Res. Int*., *80* (2009), 12, pp. 906-915
[15] Rodman, D., *et al*., Induction Hardening of Spur Gearwheels Made from 42CrMo4 Hardening and Tempering Steel By Employing Spray Cooling, *Steel Res. Int*., *82* (2011), 4, pp. 329-336

[16] Nowak, M., *et al.*, Water-Air Spray Cooling of Extruded Profiles: Process Integrated Heat Treatment of the Alloy EN AW-6082, *Journal Mater. Eng. Perform*., *22* (2013), 9, pp. 2580-2587
[17] Ma, H., *et al*., Numerical Development of Heat Transfer Coefficient Correlation for Spray Cooling in Continuous Casting, *Front. Mater*., *7* (2020), Nov., pp. 1-18
[18] Golovko, O., *et al*., Spray Cooling of Extruded EN AW-6082 Aluminum Alloy Sheets: Spatial Heat Transfer Coefficients, *Forsch. im Ingenieurwesen/Engineering Res*., *78* (2014), 3-4, pp. 131-137
[19] Chabicovsky, M., *et al*., Spray Cooling Heat Transfer above Leidenfrost Temperature, *Metals (Basel)*., *10* (2020), 9, pp. 1-16
[20] Ondrouskova, J., *et al*., Heat-Flux Computation from Measured-Temperature Histories during Hot Rolling, *Mater. Tehnol*., *47* (2013), 1, pp. 85-87
[21] Kominek, J., Pohanka, M., Estimation of the Number of Forward Time Steps For the Sequential Beck Approach Used for Solving Inverse Heat-Conduction Problems, *Mater. Tehnol.*, *50* (2016), 2, pp. 207-210
[22] Abed, A. H., *et al*., An Experimental Investigation on the Transient Heat Transfer Characteristics Using Air/Water Droplets Two-Phase Flow, *IOP Conf. Ser. Mater. Sci. Eng*., *791* (2020), 1
[23] Hadała, B., *et al*., Experimental Identification and a Model of a Local Heat Transfer Coefficient for Water--Air Assisted Spray Cooling of Vertical Low Conductivity Steel Plates From High Temperature, *Int. J. Therm. Sci*., *136* (2019), Oct., pp. 200-216
[24] Liang, G., Mudawar, I., Review of Spray Cooling – Part 2: High Temperature Boiling Regimes and Quenching Applications, *Int. J. Heat Mass Transf*., *115* (2017), Dec., pp. 1206-1222
[25] Moffat, R. J., Contributions to the Theory of Single-Sample Uncertainty Analysis, *Journal Fluids Eng. Trans. ASME*, *104* (1982), 2, pp. 250-258
[26] Li, H., *et al*., Research on the Effect of Boundary Pressure on the Boundary Heat Transfer Coefficients between Hot Stamping Die and Boron Steel, *Int. J. Heat Mass Transf*., *91* (2015), Dec., pp. 401-415
[27] Zhang, X., *et al*., Experimental Study of the Air-Atomized Spray Cooling of High-Temperature Metal, *Appl. Therm. Eng*., *71* (2014), 1, pp. 43-55
[28] Aamir, M., *et al*., Transient Heat Transfer Behavior of Water Spray Evaporative Cooling on a Stainless Steel Cylinder with Structured Surface for Safety Design Application in High Temperature Scenario, *Heat Mass Transf. und Stoffuebertragung*, *53* (2017), 2, pp. 363-375
[29] Li, H., *et al.*, High-Speed Data Acquisition of the Cooling Curves and Evaluation of Heat Transfer Coefficient in Quenching Process, *Meas. J. Int. Meas. Confed*., *41* (2008), 6, pp. 676-686
[30] Wang, H., *et al*., Experimental Study of Heat Transfer Coefficient on Hot Steel Plate during Water Jet Impingement Cooling, *Journal Mater. Process. Technol*., *212* (2012), 9, pp. 1825-1831
[31] Louhenkilpi, S., Continuous Casting of Steel, in: *Treatise on Process Metallurgy*, Elsevier, Amsterdam, The Netherlands, 2014
[32] Ye, S., *et al*., Experimental Investigation of Evaporation Dynamic of Sessile Droplets in Pure Vapor Environment with Low Pressures, *Int. J. Therm. Sci*., *149* (2020), Aug., 106213

Paper submitted: June 15, 2021
Paper revised: October 10, 2021
Paper accepted: November 6, 2021